

## Self-consistent calculations of the Zeeman splitting in metals

Anders Hjelm

*Department of Technology, Uppsala University, Box 534, S-751 21 Uppsala, Sweden*

Jean-Louis Calais

*Department of Quantum Chemistry, Uppsala University, Box 518, S-751 20 Uppsala, Sweden*

(Received 19 March 1993)

The electronic structure of metals in an external magnetic field has been investigated by means of a version of the linear-muffin-tin-orbital method, in which the magnetic field, exchange and correlation effects, and spin-orbit coupling have been included in the self-consistent iterations. The Zeeman splitting of cyclotron orbits has been calculated and compared to de Haas-van Alphen experiments for the alkali metals, the noble metals, and the platinum group metals. Also the paramagnetic susceptibilities have been calculated. Particular attention is paid to the importance of the orbital magnetic moment. A detailed treatment of palladium is included in order to evaluate the calculational method. Detailed comparisons with experimental data have been made wherever possible. In some cases the agreement between theory and experiment is very good. Possible reasons for lacking agreement are discussed and suggestions for improved theoretical procedures are made.

### I. INTRODUCTION

Investigations of the electronic structure of metals in external magnetic fields are important for our knowledge and understanding of fundamental concepts in quantum theory such as exchange, correlation, and relativistic effects. The sharpening of the conceptual tools in turn contributes to an improved interpretation of experimental data. Various experimental techniques such as susceptibility measurements, neutron diffraction, nuclear magnetic resonance, and conduction-electron-spin resonance can give information about the modifications of the electronic structure when the system is subjected to an external field. Of special importance for the band structure of metals is the de Haas-van Alphen (dHvA) effect, which directly measures the geometry of the Fermi surface. With the dHvA effect electrons in one specific cyclotron orbit on a Fermi-surface sheet can be studied. This resolution in momentum space is unique for the dHvA effect, and makes the results very suitable for comparisons with band calculations.

In systems without spontaneous polarization, i.e., diamagnetic or paramagnetic metals, the effect of the field is twofold: to split the doubly degenerate states by a certain amount of energy, the Zeeman splitting (ZS), and to induce diamagnetic currents. The ZS of cyclotron orbits on a Fermi-surface sheet can be deduced with the dHvA effect. Such investigations in the alkali metals show that the ZS is enhanced as compared to the free-electron behavior; no anisotropy can be detected, however.<sup>1-3</sup> In the noble metals the enhancement is small, but the anisotropy of the ZS is evident.<sup>4-9</sup> In the transition metals, the amount of enhancement varies, but there is always strong anisotropic behavior.<sup>10-19</sup>

These experimental findings have had no quantitative counterpart in theory. The object of the present paper is therefore to present a model that extends conventional

band calculations to include the effects of an external magnetic field. Earlier calculations of the ZS were semi-perturbational: they first established the self-consistent band structure, Fermi surface, and cyclotron orbits in zero field, and then applied the field in the last variational step (and thereby exchange and correlation effects on the ZS are not included) and calculated the cyclotron orbit  $g$  factor by a time-weighted average of the energy splitting around the nonsplit orbit.<sup>20-23</sup> We recently presented a self-consistent method based on a standard density-functional approach in the local-spin-density approximation (LSDA) to calculate the energy-band structures.<sup>24</sup> The external magnetic field is included by adding a Zeeman operator to the effective Hamiltonian, which also contains a spin-orbit coupling operator and a local exchange-correlation potential. The resulting equations are then iterated to self-consistency. No attempt is made to cover the diamagnetic effects.

In Sec. II we discuss some fundamental concepts in density-functional calculations when an external magnetic field is present. Section III treats the comparisons between dHvA experiments and calculations of the ZS. Our method of calculation is presented in Sec. IV. Using palladium as an illustration, we present in Sec. V a fairly detailed interpretation of its magnetic structure as it emerges from the combined results of theory and experiment. The calculated paramagnetic moments and estimates of the total susceptibilities are presented in Sec. VI, and the ZS of cyclotron orbits are presented and compared to experiments in Sec. VII for the alkali metals, the platinum group metals, and the noble metals.

### II. THEORY

We begin with a sketch of the fundamental framework for the theory of the electronic structure of matter in external magnetic fields. The presence of a magnetic field

carries important implications at several conceptual levels. The calculations to be described later are of density-functional type and it will therefore be natural to concentrate on such modifications of effective one-electron equations of Kohn-Sham type which will be necessary when a magnetic field is present. We start out at a more general level, however.

The Schrödinger equation,

$$\left\{ -\frac{\hbar^2}{8\pi^2m} \nabla^2 + V(\mathbf{r}) \right\} \Psi(\mathbf{r}) = E\Psi(\mathbf{r}), \quad (1)$$

for an electronic system in the absence of any external field is transformed to the following equation after the introduction of an electromagnetic field, characterized by a scalar potential  $\phi(\mathbf{r}, t)$  and a vector potential  $\mathbf{A}(\mathbf{r}, t)$  ( $e$  is the absolute value of the charge):

$$\left\{ \frac{1}{2m} \left[ -\frac{i\hbar}{2\pi} \nabla + \frac{e}{c} \mathbf{A} \right]^2 + V + \phi \right\} \Psi(\mathbf{r}) = E\Psi(\mathbf{r}). \quad (2)$$

The electric field  $\mathbf{E}$  and the magnetic field (strictly speaking the magnetic induction)  $\mathbf{B}$  are related to these potentials in the following way:

$$\mathbf{E} = -\nabla\phi - \frac{1}{c} \frac{\partial \mathbf{A}}{\partial t}; \quad \mathbf{B} = \nabla \times \mathbf{A}. \quad (3)$$

The fields are invariant under gauge transformations of the potentials:

$$\mathbf{A}' = \mathbf{A} - \nabla\chi; \quad \phi' = \phi + \frac{1}{c} \frac{\partial \chi}{\partial t}. \quad (4)$$

For the wave function the gauge transformation means multiplication by a phase factor:

$$\Psi'(\mathbf{r}) = \Psi(\mathbf{r}) \exp \left[ -\frac{ich}{2\pi c} \chi(\mathbf{r}) \right]. \quad (5)$$

Neither the wave function nor the potentials are measurable. Quantities which are measurable must however be invariant under gauge transformations, and to ensure that invariance must be the primary requirement in all theories of the electronic structure of matter in electromagnetic fields.

Spin obviously plays a central role in magnetic problems. Instead of the Schrödinger equations (1) or (2) we should discuss the corresponding Dirac equations either in their fully relativistic four-component form or in the corresponding nonrelativistic two-component Pauli approximation. Löwdin<sup>25</sup> has used a partitioning technique to go from four to two components. That paper which also contains a very clear discussion of spin-orbit coupling and contact interactions including the role of gauge invariance constitutes a good starting point for any treatment of matter in electromagnetic fields.

Another general aspect which should be kept in mind concerns the connection between many- and one-electron functions and equations. To combine relativity and many-particle quantum mechanics is obviously one of the great problems of the century and this is not the place for it. But even though we work with one-electron equations it does not hurt to remember that—as in the nonrela-

tivistic case—there should be a many-electron equation and a many-electron wave function at the start of the quantum-mechanical treatment of the problem. Density-functional theory circumvents this aspect and as we are primarily going to work within the framework of that theory we will not have to dwell more on this question here.

The use of density-functional theory for systems in magnetic fields has recently been surveyed in a very thorough way by Vignale, Rasolt, and Geldart.<sup>26</sup> They show how the role of the number density of the ordinary density-functional theory must be taken over by the spin and current densities when a magnetic field is present. The effects of spin polarization were incorporated relatively early into what became spin-density-functional theory,<sup>27</sup> but the influence of the orbital current density has only recently been taken into account.<sup>28,29</sup> The generalized Hohenberg-Kohn theorem which is applicable in the magnetic case states that the external scalar and vector potentials as well as the nondegenerate ground-state wave function are uniquely determined by the density distributions  $n(\mathbf{r})$  and  $\mathbf{j}_p(\mathbf{r})$ . Here  $n(\mathbf{r})$  is the number density, i.e., the ground-state expectation value of the number density operator.

$$n^{\text{op}}(\mathbf{r}) = \Psi^+(\mathbf{r})\Psi(\mathbf{r}). \quad (6)$$

The paramagnetic current density  $\mathbf{j}_p(\mathbf{r})$  is the ground-state expectation value of the corresponding operator:

$$\mathbf{j}_p^{\text{op}}(\mathbf{r}) = -\frac{i\hbar}{8\pi m} \{ \Psi^+(\mathbf{r})\nabla\Psi(\mathbf{r}) - [\nabla\Psi^+(\mathbf{r})]\Psi(\mathbf{r}) \}. \quad (7)$$

This term, *paramagnetic current density*, is used to distinguish it from the *diamagnetic current density*,

$$\frac{e}{mc} n(\mathbf{r}) \mathbf{A}(\mathbf{r}). \quad (8)$$

Together these two components form the orbital current density, also called physical current density by Vignale *et al.*,

$$\mathbf{j}(\mathbf{r}) = \mathbf{j}_p(\mathbf{r}) + \frac{e}{mc} n(\mathbf{r}) \mathbf{A}(\mathbf{r}). \quad (9)$$

This physical current density  $\mathbf{j}(\mathbf{r})$  and the number density  $n(\mathbf{r})$  are gauge invariant, but the paramagnetic current density  $\mathbf{j}_p(\mathbf{r})$  is *not gauge invariant*. That obviously creates serious conceptual difficulties, which Vignale and Rasolt have managed to overcome, however. An essential aspect of that problem is the fact that the exchange-correlation potential  $E_{\text{XC}}$  is a functional of the gauge-invariant combination

$$\nabla \times \left[ \frac{\mathbf{j}_p(\mathbf{r})}{n(\mathbf{r})} \right]. \quad (10)$$

The Kohn-Sham type of one-electron equation associated with the orbital current density derived by Vignale and Rasolt is of the form

$$\left\{ -\frac{\hbar^2}{8\pi^2 m} \nabla^2 - \frac{i\hbar e}{4\pi m c} [\mathbf{A}_{\text{eff}}(\mathbf{r}) \cdot \nabla + \nabla \cdot \mathbf{A}_{\text{eff}}(\mathbf{r})] + \frac{e^2}{2m c^2} \mathbf{A}^2(\mathbf{r}) + V(\mathbf{r}) + V_H(\mathbf{r}) + V_{\text{XC}}(\mathbf{r}) \right\} \Psi_i = \epsilon_i \Psi_i . \quad (11a)$$

Here the effective vector potential is the sum of the “actual” vector potential  $\mathbf{A}(\mathbf{r})$  and the functional derivative of  $E_{\text{XC}}$  with respect to  $\mathbf{j}_p(\mathbf{r})$ :

$$\mathbf{A}_{\text{eff}}(\mathbf{r}) = \mathbf{A}(\mathbf{r}) + \mathbf{A}_{\text{XC}}(\mathbf{r}) . \quad (11b)$$

Similarly, the three scalar potential terms in (11a) are the “external” potential due to the nuclei, the Hartree term, and the exchange-correlation term.

Vignale and Rasolt prove that this one-electron equation (11a) is indeed gauge invariant. For applications to crystals with translational symmetry that statement is decisive, since it ensures that the density, the current density, the effective scalar potential, and the exchange-correlation part of the effective vector potential are all periodic. All the usual theorems for the classification of the solutions of (11a), according to the representations of the magnetic translation group, are therefore valid.<sup>30</sup>

Combined with suitable modifications due to spin the equation of Vignale and Rasolt, (11a), provides a general framework for applying density-functional theory to magnetic problems. In our own calculations an operator,

$$\mu_B \mathbf{B} \cdot (\mathbf{I} + 2\mathbf{s}) , \quad (12)$$

is included in the self-consistent treatment. The orbital part of (12) is obtained from the terms  $\mathbf{A} \cdot \nabla + \nabla \cdot \mathbf{A}$  in (11a), in such cases when it is possible to define an orbital angular momentum  $\mathbf{I} = (2\pi/\hbar) \mathbf{r} \times \mathbf{p}$ . Strictly speaking that is possible only for free atoms and ions. In a method like the linear-muffin-tin-orbital (LMTO) method, with muffin-tin spheres as a basic notion, a similar formulation can, however, be defended.

Finally, a word should be said about the use of density-functional theories in treatments of the de Haas–van Alphen effect. Recently, Serene<sup>31</sup> has developed the theory of this effect within the framework of the current-density-functional theory of Vignale and Rasolt. Serene discusses a number of rather subtle points which cannot be disregarded in the interpretations of de Haas–van Alphen experiments. In particular, he asks the essential question of whether the de Haas–van Alphen effect can be treated in the framework of density-functional theory. Perhaps his most important result is that any local approximation to the Vignale-Rasolt current-density-functional theory can at best yield de Haas–van Alphen oscillations associated with the Kohn-Sham band structure. That statement, which does not sound too revolutionary, needs a few comments. Part of the background is a paper by Mearns<sup>32</sup> in which it is shown that the Kohn-Sham Fermi surface is different from what Mearns calls the quasiparticle Fermi surface. The latter is what is obtained in principle from the full many-body problem, in other words the Dyson equation,

and should therefore also be identical to the experimental result. According to Serene, the correct de Haas–van Alphen oscillations are contained in the Vignale-Rasolt exchange-correlation functional. Any differences between the “quasiparticle” results and a Kohn-Sham calculation must be due to the highly nonlocal character of that exchange-correlation functional.

### III. COMPARISONS OF ZEEMAN SPLITTING FROM dHvA EXPERIMENTS AND THEORY

The de Haas–van Alphen effect, an oscillatory contribution to the total magnetization as a function of applied field, carries information about the electrons at the Fermi surface. The oscillations arise as subsequent Landau tubes pass through the Fermi surface, and are periodic in the reciprocal field. The frequency is proportional to the extremal cross-sectional area of the Fermi surface perpendicular to the magnetic field. In an external magnetic field, the Fermi surface is slightly split, giving rise to two almost identical cross-sectional areas,  $A_1$  and  $A_2$ . This will appear as a modulation of the dHvA amplitude with a cosine function (the spin-splitting factor) with the argument

$$\pi R = \pi \frac{\hbar}{2\pi e} \frac{A_1 - A_2}{B} , \quad (13)$$

where  $B$  is the magnetic-field strength. In the rigid-band approximation the difference in area in the equation above can be expressed in terms of the energy difference between the split cyclotron orbits on  $\mathbf{k}$  states confining the zero-field areas, by introducing the cyclotron orbit effective mass  $m_c$  (expressed in units of the free-electron mass). The energy difference is described by a proportionality factor, the cyclotron orbit  $g$  factor,  $g_c$ . The relation will then be

$$R = \frac{g_c m_c}{2} . \quad (14)$$

By careful measurements of the dHvA amplitude the angular variation of the spin-splitting factor for specific Fermi-surface sheets can be obtained. When solving for  $R$  or  $g_c$  there will be an unknown integer in the expression, as an inverse cosine function is solved. Therefore, the experimental results describe the anisotropy, but not the absolute value, of  $R$  or  $g_c$ . Estimates of the values of  $R$  or  $g_c$  can be made from the bulk susceptibility. They can, however, vary considerably from one Fermi-surface sheet to another. An extensive review of the dHvA effect and applications has been written by Shoenberg.<sup>33</sup>

The argument of the spin-splitting factor,  $R$ , is exchange enhanced but not renormalized from electron-phonon interaction.<sup>34</sup> In the literature two different approaches regarding the electron-phonon effect have been made. The first one treats both  $g_c$  and  $m_c$  as if they were unaffected by electron-phonon effects, and directly comparable to bare band quantities. This means that the evaluation of  $g_c$  from experiments relies on calculated values of the mass. On the other hand, as the band structure in the vicinity of the Fermi level is distorted from the phonon interaction, the second approach uses the ex-

perimentally determined masses, and  $g_c$  will be decreased by the same amount as  $m_c$  is enhanced (compared to bare band values).<sup>18</sup> The values of  $g_c$  obtained in this way only depend on experimental data, and describe the physical situation. In the present paper, comparisons between experiments and calculations are concentrated on studies of  $R$ , as this removes the uncertainty whether the data should be electron-phonon compensated or not. This, together with the self-consistency, implies that theory and experiments are directly comparable in the present paper, in contrast to earlier calculations,<sup>20-23</sup> where the comparisons included the unknown factors from electron-phonon interaction as well as exchange-correlation enhancement. It is also advantageous to study  $R$  as this quantity is closer to experimental raw data.

The calculations presented later do not include Landau condensation in the calculational scheme. However, the number of Landau tubes inside the Fermi-surface sheets is large at laboratory fields, except for small sheets like the  $X$ -centered hole pockets in the late transition metals. This means that the distribution of Landau tubes may be regarded as quasicontinuous and will cause no conflict with the conventional distribution of states in  $\mathbf{k}$  space.

#### IV. METHOD OF CALCULATION

The basic method used for calculating the self-consistent, spin-polarized band structures was the LMTO-ASA (atomic-spheres-approximation) method in the scalar relativistic approximation, and the local-spin-density approximation.<sup>35</sup> In the self-consistent-field calculation, an effective exchange-correlation (XC) potential was used, as well as the orbital polarization (OP) correction.<sup>36,37</sup> To the variational step the spin orbit (SO) and Zeeman ( $H_z = \mu_B \mathbf{B} \cdot [l + 2s]$ ) operators were added. In the calculations the XC potential by von Barth and Hedin,<sup>38</sup> OP correction, combined correction terms, and orbitals of  $s$ ,  $p$ , and  $d$  symmetry were included, except when otherwise stated.

In a cubic system with a preferred direction of magnetization the irreducible part of the Brillouin zone is generally  $\frac{1}{4}$ .<sup>39</sup> Therefore, the integration over  $\mathbf{k}$  states was performed over an appropriate part of the zone, with a density of  $\mathbf{k}$ -points corresponding to 505 points per  $\frac{1}{48}$  for the fcc structure and 506 points for the bcc metals. The direction of quantization, the  $z$  axis in the calculations, was transformed from the crystal coordinate system to be aligned with the external magnetic field. Convergence for each field strength and field direction was monitored by studying the gravity centers for the spin,  $l$  and  $m_l$  projected bands,  $E_v$ . The convergence criterion was that no single  $E_v$  should shift more than  $15 \mu\text{Ry}$  between two successive iterations, and the rms value of the shifts of the  $E_v$ 's should not be more than  $10 \mu\text{Ry}$ .

When convergence was achieved, the spin and orbital magnetic moments were calculated as described by Brooks and Kelly.<sup>40</sup> The susceptibility was obtained by dividing the corresponding magnetization with the applied field.

The split Fermi-surface areas were calculated in a field of 10 T by varying the length of the wave vector in a

specific direction until the eigenvalue for the  $\mathbf{k}$  point and band in question coincided with the Fermi energy, with an accuracy of  $1 \mu\text{Ry}$ . The areas were then obtained by integration of the Fermi wave vectors around the orbit with an angular step of  $2.5^\circ$ .  $m_c$  was calculated using the relation

$$m_c = \int_0^{2\pi} |\mathbf{k}_F| (\hat{\mathbf{k}}_F \cdot \mathbf{v}_\perp)^{-1} d\phi_c,$$

where the differentiation was solved numerically by

$$\hat{\mathbf{k}}_F \cdot \mathbf{v}_\perp \approx \frac{E(\mathbf{k}_F + \Delta\mathbf{k}) - E(\mathbf{k}_F - \Delta\mathbf{k})}{2\Delta k},$$

with  $|\Delta\mathbf{k}| = 10^{-4} 2\pi/a$  in the same direction as the Fermi wave vector.  $R$  and  $g_c$  were then calculated using Eqs. (13) and (14).

In the calculations of anisotropic properties the magnetic-field direction was varied in the symmetry planes. For all graphs presenting data with cubic symmetry ( $\Gamma$ -centered Fermi-surface sheets) the field starts in the [001] direction and is then moved towards [110] in the  $(1\bar{1}0)$  plane (cf. Fig. 1). The following part of the diagrams presents data for the field aligned with the (001) plane, from [110] towards [100]. As the  $(0\bar{1}1)$  plane and  $(1\bar{1}0)$  plane are equivalent the irreducible part of the unit sphere (the shaded area in Fig. 1) is included. For the  $X$ -centered hole pockets in the late transition metals the irreducible part is  $\frac{1}{16}$ , as shown in Fig. 1. For these calcu-

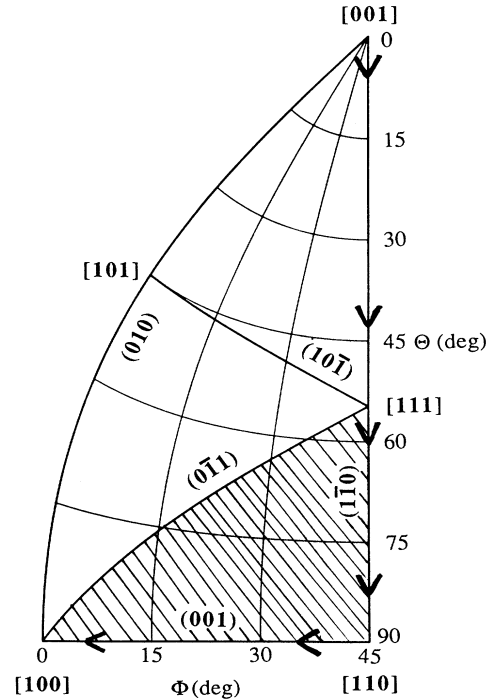


FIG. 1.  $\frac{1}{16}$  of the unit sphere is shown, the irreducible part for an  $X$  centered Fermi-surface sheet in a cubic symmetry. The shaded area corresponds to the irreducible  $\frac{1}{48}$  for a Fermi-surface sheet centered at the  $\Gamma$  point in a cubic structure. In the calculations the field direction is varied according to the arrows.

lations the field is applied in the same directions, but the symmetry is expanded by studying the Fermi-surface sheets located at the three different  $X$  point orientations. However, data for the nonsymmetry  $(0\bar{1}1)$  and  $(10\bar{1})$  planes are not included in the figures, which present only the  $(010)$ ,  $(001)$ , and  $(1\bar{1}0)$  planes.

In order to estimate the general accuracy of the calculated band structures, extremal Fermi-surface areas can be compared to experiments. The accuracy of the calculated Fermi-surface area can be expressed as the shift of the Fermi level that is required to bring the calculated ( $A_{\text{calc}}$ ) and experimental ( $A_{\text{exp}}$ ) areas to agree,

$$\Delta E = \frac{A_{\text{exp}} - A_{\text{calc}}}{\pi m_c},$$

where  $m_c$  is the calculated cyclotron orbit mass in units of the free-electron mass.

For the alkali metals the calculated Fermi surfaces are too large, with smaller errors in Na, K, and Rb (around 1.2 mRy) than in Li (6.0 mRy). Regarding Cs, cf. Sec. VII and Ref. 23. In the late transition metals investigated here the error is always smaller than 10 mRy. The largest value, 9.4 mRy, is found for the  $\Gamma 5$  surface in Ir, which is a very anisotropic Fermi-surface sheet. In the noble metals the errors are quite small, except for the neck orbits where the errors are around 10 mRy. Thus the overall agreement is satisfactory. Regarding the validity and accuracy of Fermi-surface areas calculated from local-density-approximation methods, there is an overwhelming amount of papers published where the results in general are similar to the present work. Of particular interest are the papers by Ahuja and co-workers where the influence of the choice of XC potential on the Fermi-surface areas is studied.<sup>41-43</sup>

## V. PALLADIUM

Palladium is a system with strong exchange enhancement of the magnetization, and effects of spin-orbit coupling are also evident. Therefore, palladium is used for interpretation of the model in the present paper, and the results are discussed in some detail. Thereafter, the results for other metals are presented in a more descriptive manner.

The effect of the spin part of the Zeeman Hamiltonian is to create a spin polarization of the conduction electrons, where the magnetic spin moment is determined in balance with the XC potential through the self-consistency. The obtained moment for Pd, without SO coupling and without the orbital term in  $H_Z$ , in an external field of 10 T is presented in Table I. When the orbital part of  $H_Z$  is added an orbital magnetic moment is also created while the spin moment is unaffected (cf. Table I). If SO coupling is included and only the spin term in  $H_Z$  considered, the spin moment drops and an orbital moment, induced by the SO coupling as in spontaneous spin-split metals, is developed. Finally, inclusion of the orbital operator increases the spin moment somewhat via the SO interaction, and the orbital moments from the

TABLE I. Calculated spin and orbital magnetic moments for palladium (in units of Bohr magnetons per atom) in an external field of 10 T in a  $[001]$  direction, calculated without using the OP correction.

Spin-orbit interaction	Zeeman operator	$\mu_s$	$\mu_l$
No	spin only	0.0134	0.0000
No	spin and orbit	0.0134	0.0008
Yes	spin only	0.0080	0.0008
Yes	spin and orbit	0.0092	0.0016

Zeeman operator and SO coupling are roughly added. Thus, the magnetic moments depend on the interaction between the Zeeman operator, SO coupling, and XC enhancement, and self-consistency is required in order to have correct results.

The effect on the calculated magnetic moments of using different XC potentials is presented in Table II, where also the difference when  $f$  orbitals are included is indicated. The potential by von Barth and Hedin<sup>38</sup> (BH) gives the lowest magnetization, while using it with Janak parameters<sup>44</sup> (BHJ) gives the largest moments, together with the Gunnarsson-Lundqvist potential<sup>45</sup> (GL). For Pd, the XC potential giving a susceptibility nearest the experiment value ( $10.5 \times 10^{-4}$ ), is the Vosko-Wilk-Nusair potential<sup>46</sup> (VWN).

By comparing the last row of Table I and the first row in Table II one can see that the effect of the OP correction is to increase the spin moment from  $0.0092\mu_B$  per atom to  $0.0094\mu_B$  per atom, and from  $0.0016\mu_B$  per atom to  $0.0019\mu_B$  per atom for the orbital part. Thus, OP is a quite small correction to the system.

In palladium, and also in platinum, the calculated bulk magnetization shows an anisotropy of about 2%. The variation is near the numerical noise level, but at least in Pd the anisotropic behavior is evident. The magnetization in Pd has a maximum when the field is in a  $[001]$  direction, and minima in the  $[110]$  directions. For platinum, the minimum appears to be in the  $[111]$  direction. The anisotropy originates from the spin part of the magnetic moment, which is in contrast to the anisotropy in ferromagnetic metals, where usually the orbital part of the magnetic moment is anisotropic and the spin moment isotropic.<sup>47</sup>

Regarding the Zeeman Splitting (ZS) of cyclotron or-

TABLE II. Calculated magnetic moments for Pd in external field of 10 T in a  $[001]$  direction. OP and  $f$  orbitals are included, except in the first row where orbitals up to  $d$  have been used. The last column displays the corresponding SI susceptibilities.

Potential	$\mu_s$	$\mu_l$	$\chi$ ( $10^{-4}$ )
BH <i>spd</i>	0.0094	0.0019	8.9
BH	0.0097	0.0019	9.2
BHJ	0.0144	0.0025	13.4
VWN	0.0124	0.0022	11.5
GL	0.0141	0.0024	13.1

bits anisotropic effects are large. The major part of the anisotropy is created by SO coupling and it is magnified by the XC enhancement. (The effect of SO coupling on the ZS is well described in Ref. 20.) In Figs. 2, 3, and 4 the influence of different XC potentials on the ZS for the  $\Gamma_6$  sheet,  $\alpha_5$  orbit, and  $X_4$  pocket in Pd is studied, by using the BH and VWN potentials, respectively. The effect of the different XC potentials is roughly to scale the ZS with the total magnetization, and the anisotropic behavior is slightly modified. However, as the ZS is larger when using the VWN potential than when using the BH potential, the anisotropy is consequently larger, and the agreement with experiments is better for the VWN potential than for the BH potential, at least for the  $\Gamma_6$  sheet and the  $\alpha_5$  orbit. This is also consistent with the previous statement that the VWN potential gives the most accurate value of the magnetization in palladium. In Figs. 2–4 the influence of OP on the anisotropy of the ZS also is presented. There is no substantial contribution to the anisotropy from OP, there is just a uniform increase of the polarization.

The contribution from spin and orbital moments and XC effects to the ZS on cyclotron orbits have been analyzed by calculating the ZS using the fully self-consistent potential, but neglecting spin and/or orbital parts of the Zeeman Hamiltonian. This procedure projects out the various contributions to the self-consistent state. The XC enhancement factor is determined as the ratio between the fully self-consistent value of  $g_c$  and the value obtained when the contribution from XC splitting is subtracted. The spin and orbital components are then multiplied by this factor in order to divide  $g_c$  into spin and orbital parts. As seen in Fig. 5, the XC enhancement on the  $\Gamma_6$  sheet is approximately 6 with a small increase in the [110]

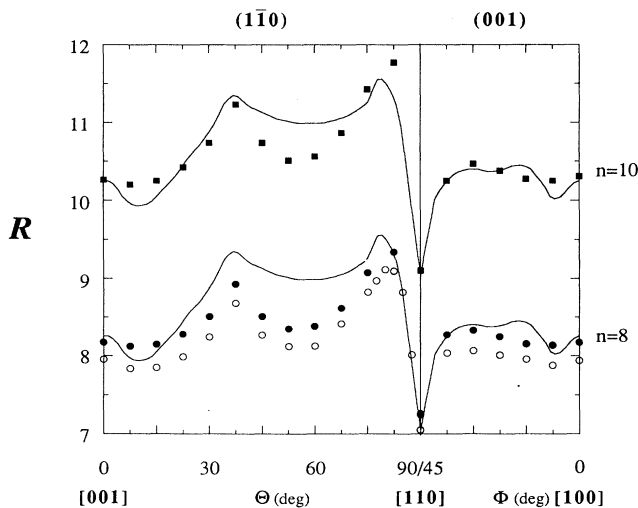


FIG. 2.  $R$  for cyclotron orbits on the extremal Fermi-surface areas perpendicular to the direction of the external magnetic field for the  $\Gamma_6$  sheet in Pd as a function of field direction, calculated with the BH potential, with (solid circles) or without (empty circles) OP, and with the VWN potential and OP (solid squares). The experimental data (Ref. 14) (solid lines) are displayed for two choices of the arbitrary integer,  $n = 8$  and 10.

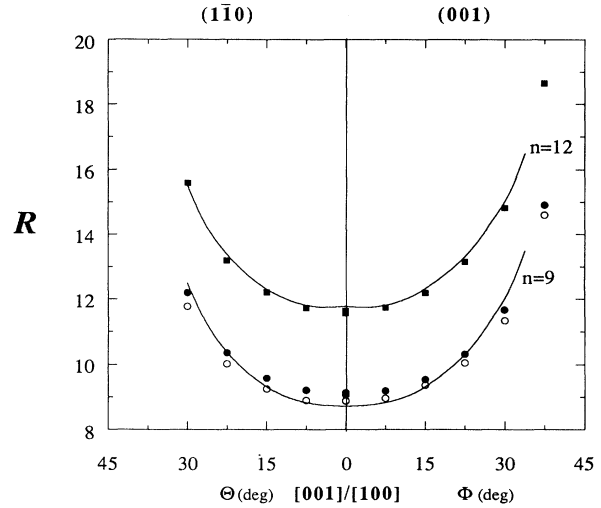


FIG. 3. Same as the preceding figure, but for the  $\alpha$  orbit in palladium. The integers used in the plot of the experimentally determined anisotropy (Ref. 14) are 9 and 12.

direction, and the orbital contribution to  $g_c$  is about 20%. On the  $\alpha$  orbit  $g_c$  and its components are almost isotropic. The enhancement factor is approximately 6 as for the  $\Gamma_6$  sheet, and the orbital contribution to  $g_c$  is 8%. On the  $X$ -centered hole pocket,  $X_4$ , presented in Fig. 6, the situation is more dramatic. When the field is near a [001] direction, the orbital moment is negative and very large, and the XC enhancement factor is also large. The reasons for obtaining a reversed orbital moment in some parts of the Brillouin zone are not evident.

The magnetic structure of Pd in external fields has also been studied by neutron diffraction.<sup>48</sup> In the present work, the magnetic form factors were calculated, using the dipole approximation,<sup>49</sup> and compared to the experi-

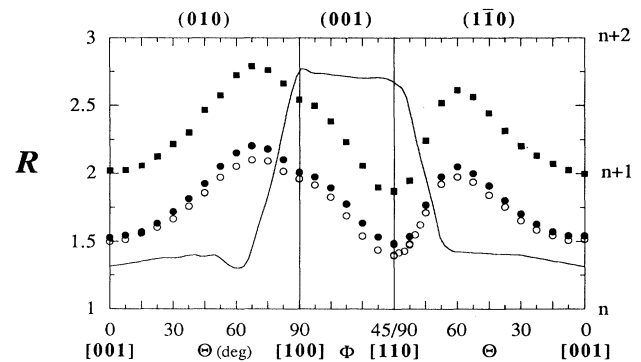


FIG. 4. Zeeman splitting on the  $X_4$  hole pocket in Pd, calculated with the BH potential (circles) and with (filled) and without (empty) OP, as well as the VWN potential and OP (squares). The solid line represents the experimental anisotropy, and is plotted with the unknown integer equal to 1, although measurements of the phase at infinite field excluded odd values of  $n$  (Ref. 15).

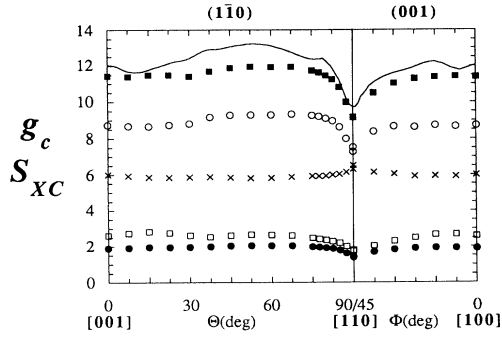


FIG. 5. The cyclotron orbit  $g$  factor for the  $\Gamma_6$  Fermi surface sheet in Pd. The experimental values (Ref. 14) (solid line) are obtained with the arbitrary integer equal to 8, and have been compensated for the electron-phonon interaction in order to be comparable with the bare band  $g$  factors. Calculated values are presented with (solid squares) and without (solid circles) XC enhancement. The enhancement factor, obtained as a ratio between the two, is marked with crosses. The  $g_c$  factor has also been divided into its spin (empty circles) and orbital (empty squares) components.

mental ones in Fig. 7. For the three innermost reflections the agreement is very good, but the lack of asphericity in the calculations gives worse agreement for larger  $q$  vectors. The calculated (using the VWN potential,  $f$  orbitals and OP) magnetic moment at 5.72 T, the field strength used in the experiment, is  $0.0083\mu_B$ , in good agreement with the experimental moments of  $0.0075\mu_B$  and  $0.0080\mu_B$  for the two different samples. In connection to this the spin and charge densities of the conduction electrons were calculated. As can be seen in Fig. 8 the spin density is much more contracted than the charge density. A similar treatment for the ferromagnetic transition metals gives worse agreement in form factor than for Pd, since the calculated spin density is not as contracted as the experiments indicate. In this context it is adequate to

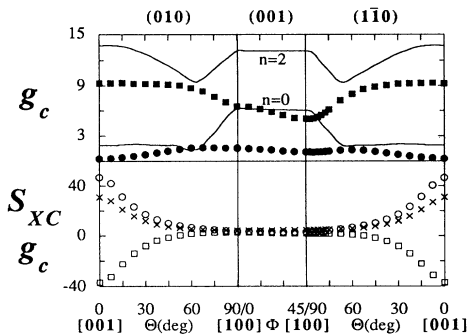


FIG. 6. The upper panel shows the  $g_c$  factors on the X4 hole pocket in Pd, calculated with (solid squares) and without (solid circles) XC enhancement. Two possible alternatives for  $g_c$  from experiments (Ref. 15) (compensated for electron-phonon interaction) are also displayed (solid lines). The lower panel shows the XC enhancement factor (cross) and the spin (circles) and orbital (squares) contributions to the Zeeman splitting.

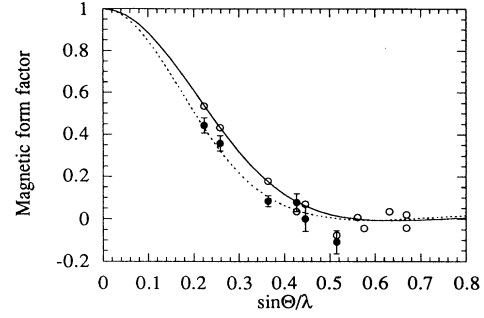


FIG. 7. The calculated (lines) and experimental (Refs. 48 and 50) (circles) magnetic form factors for Pd (open symbols and solid line) and Pt (filled symbols and dashed line). The experimental errors for Pd have not been marked in the figure as they are of comparable size to the plot symbols.

also present the magnetic form factor for Pt (Fig. 7), taking the experimental data from Ref. 50.

## VI. SUSCEPTIBILITY

The magnetic susceptibility  $\chi$  relates the magnetization density  $M$  of a system to the magnetic field  $H$  responsible for that magnetization. In general  $\chi$  depends on the field, even though in the most commonly studied case the magnetization varies linearly with the field so that the susceptibility is constant with respect to the field. The susceptibility can also be expressed in terms of the Helmholtz free energy  $F$  (see, e.g., Ref. 51, Chap. 31). We thus have

$$\chi = \frac{\partial M}{\partial H} = -\frac{1}{V} \frac{\partial^2 F}{\partial H^2}. \quad (15)$$

At  $T=0$  the Helmholtz free energy  $F$  reduces to the ground-state energy  $E_0$ . Then the magnetization density can be written as

$$M = -\frac{1}{V} \frac{\partial E_0}{\partial H}. \quad (16)$$

For metals, attempts at calculating the magnetic susceptibility have focused on three contributions: the

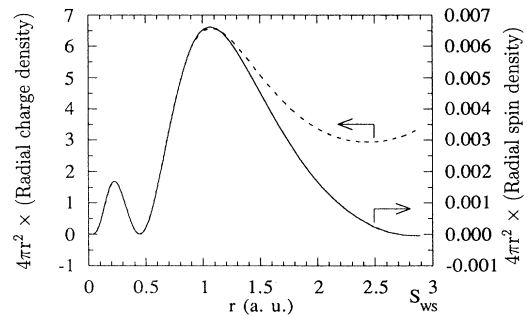


FIG. 8. Spin (solid line) and charge (dashed line) densities of the band electrons in Pd, multiplied by  $4\pi r^2$ , calculated in a field of 5.72 T.

paramagnetic Pauli susceptibility, which is obtained from considering only the spin magnetic moments of the electrons in an electron gas, the Landau diamagnetic susceptibility due to the orbital effects of the electrons, and the Larmor diamagnetic susceptibility due to the closed ion core shells.

A more complete calculation of the magnetic susceptibility should start—at least in principle—with (16). From the total energy in the ground state of the system as a function of the magnetic field, one gets the magnetization density from (16) and the susceptibility from (15). In band calculations of LMTO type that program can be carried out by calculating spin and orbital contributions to the magnetization density in each sphere from all occupied wave functions.<sup>40,52</sup> The results are then integrated over all occupied energies and over all spheres. Such calculations are done only to first order in the magnetic field and the resulting susceptibility, which is dominating, therefore corresponds to the Pauli paramagnetic contribution.

The Larmor diamagnetic contribution to the susceptibility is calculated from the formula

$$\chi_{\text{dia core}} = -ZN \frac{e^2}{6m} \langle r^2 \rangle,$$

where  $N$  is the number of atoms per unit volume and the expectation value  $\langle r^2 \rangle$  is calculated from the ion core charge density.

To calculate the Landau diamagnetic contribution to the susceptibility is a considerably more difficult task, as discussed by Misra and Roth.<sup>53</sup> In a free-electron system it equals  $-\frac{1}{3}$  of the Pauli spin susceptibility (see, e.g., Ref. 54, pp. 144–149). For the alkali metals where it is possible to use a pseudopotential method, Misra and Roth<sup>53</sup> have calculated the Landau diamagnetic susceptibility. Their results did not differ very much from the free-electron values, however. For the noble metals copper and silver, Svechkarov, Poltoratskii, and Mar'yanina have presented calculations of the magnetic susceptibility including the diamagnetic contribution.<sup>55</sup> Their calculations are based on a band structure obtained from a free-electron approximation complemented with perturbations from the main Bragg planes. To our knowledge, no calculations of the diamagnetism of the conduction electrons in a transition metal have been performed.

#### A. Alkali metals

For the alkali metals the magnetic moments are of almost pure spin character, as expected from the dominant  $s$  character of the eigenfunctions. The paramagnetic susceptibilities, derived from the calculated magnetic moments using different XC potentials, are presented in Table III together with the Pauli susceptibility [ $\mu_0 \mu_B^2 D(E_F)$ , where  $D(E_F)$  is the density of states at the Fermi level]. Generally the BH and VWN potentials give smaller magnetizations than the BHJ potential does, and the GL potential gives the largest magnetic moments. The calculated diamagnetic susceptibility of the ion cores, the diamagnetic susceptibility for the conduction

TABLE III. Calculated SI susceptibility of the alkali metals, derived from the magnetic moments in an external field of 10 T in a [001] direction, using different XC potentials. The unenhanced Pauli spin susceptibility (proportional to the density of states at the Fermi level) is also presented.

Metal	SI susceptibility ( $10^{-5}$ )				Pauli
	BH	BHJ	VWN	GL	
Li	3.0	3.6	3.1	3.9	1.55
Na	1.4	1.5	1.4	1.6	0.84
K	1.3	1.5	1.2	1.5	0.71
Rb	1.2	1.5	1.2	1.5	0.68
Cs	2.2	3.2	2.0	3.2	0.89

electrons, as calculated by Misra and Roth,<sup>53</sup> and the total susceptibility, i.e., the sum of the three contributions previously discussed, using the value calculated with the BH potential, are presented in Table IV. As a final comparison the experimentally determined susceptibilities are displayed.

As seen in Table IV, the susceptibilities of Li and Cs are overestimated, whereas the agreement is very good for Na, K, and Rb. The situation for Cs will be discussed later in the present paper.

#### B. Platinum group metals

The magnetic moments for Rh, Pd, Ir, and Pt in an external field of 10 T have been calculated and are presented as susceptibilities in Table V. The orbital contribution to the total magnetic moment is large, in order of half of the total magnetization (see Table VI), as  $d$  states give large moments from the orbital part of the Zeeman Hamiltonian (cf. the discussion below). For Pd, however, the spin enhancement is so large that the relative contribution from the orbital moment is lower, 17%. In order to compare with experimental susceptibilities an estimate of the Landau diamagnetism has to be used. In this case a correspondence to the free-electron value is used, one-third of the Pauli spin susceptibility. However, the diamagnetic corrections are quite small compared to the paramagnetic contribution in these metals. The comparison is presented in Table VII. All XC potentials underestimate the susceptibility in Pt, and overestimate it in Ir, while Rh shows good agreement with experiments.

TABLE IV. Estimated total susceptibilities for the alkali metals from the present calculation are compared to experimental values. The first two columns show the diamagnetic corrections to the calculated susceptibility from the ion core and the conduction electrons (CE).

Metal	SI susceptibility ( $10^{-5}$ )			Expt.
	core	dia CE <sup>a</sup>	Tot BH	
Li	-0.08	-0.29	2.7	1.4
Na	-0.29	-0.26	0.81	0.85
K	-0.46	-0.22	0.57	0.57
Rb	-0.61	-0.20	0.43	0.38
Cs	-0.77	-0.18	1.2	0.52

<sup>a</sup> Reference 53.

TABLE V. Calculated susceptibility for Rh, Pd, Ir, and Pt obtained from the magnetic moments using four different XC potentials and a magnetic field of 10 T in a [001] direction. The Pauli spin susceptibility as calculated from the density of states at the Fermi level is also presented.

Metal	SI susceptibility ( $10^{-4}$ )				Pauli
	BH	BHJ	VWN	GL	
Rh	2.1	2.2	2.2	2.2	0.63
Pd	8.9	12.9	11.1	12.7	1.1
Ir	1.5	1.5	1.5	1.5	0.44
Pt	2.9	3.1	3.0	3.1	0.80

TABLE VI. The amount of orbital contribution to the total paramagnetic moment for some of the late transition metals and the noble metals, as calculated in the present work.

Metal	Relative orbital moment (%)
Rh	47
Pd	17
Ir	55
Pt	31
Cu	53
Ag	37
Au	53

TABLE VII. The calculated diamagnetic components to the susceptibility from the core electrons and the conduction electrons (CE) are shown, and also the total estimated susceptibility using the BH potential. Finally, experimental data are presented.

Metal	SI susceptibility ( $10^{-4}$ )			Expt.
	core	dia CE <sup>a</sup>	Tot. BH	
Rh	-0.16	-0.21	1.8	1.7
Pd	-0.14	-0.37	8.4	10.5
Ir	-0.25	-0.15	1.1	0.38
Pt	-0.22	-0.27	2.4	3.0

<sup>a</sup>Minus one-third of the Pauli spin susceptibility.

TABLE VIII. Calculated susceptibilities for the noble metals, as in previous tables.

Metal	SI susceptibility ( $10^{-5}$ )				Pauli
	BH	BHJ	VWN	GL	
Cu	4.3	4.4	4.3	4.4	1.7
Ag	2.1	2.1	2.0	2.1	1.0
Au	2.9	3.0	3.0	3.0	1.2

TABLE IX. Diamagnetic corrections and the estimates of the total susceptibilities for the noble metals.

Metal	SI susceptibility ( $10^{-5}$ )			Expt.
	core	dia CE	Tot. BH	
Cu	-0.79	-0.89 <sup>a</sup>	2.6	-0.96
Ag	-1.1	-0.28 <sup>a</sup>	0.64	-2.4
Au	-1.8	-0.39 <sup>b</sup>	0.78	-3.4

<sup>a</sup>Reference 55.

<sup>b</sup>Minus one-third of Pauli spin susceptibility.

### C. Noble metals

The magnetic moments in the noble metals are small, and therefore more difficult to calculate. Numerical noise and uncertainties in the model can produce large relative errors. As can be seen in Tables VIII and IX the calculated susceptibility is exaggerated for the noble metals. This can be due to two reasons.

(i) The calculated paramagnetic moments are too large.

(ii) The diamagnetic corrections are underestimated. Svechkarev, Poltoratskii, and Mar'yanina<sup>55</sup> have calculated the total susceptibility of copper and silver. Their values of the the diamagnetic contribution from the conduction electrons are slightly larger than one-third of the Pauli susceptibility in Cu, while it is somewhat smaller in Ag. This might indicate that the diamagnetism can be unexpectedly large, but not large enough to explain the discrepancies in the present paper. Studies of the ZS over the Fermi surfaces, presented in a later section, indicate that the first error is present but not at such a large amount as to exclude the second source of error.

## VII. ZEEMAN SPLITTING OF CYCLOTRON ORBITS

### A. Alkali metals

Many local-density-approximation (LDA) calculations fail in reproducing the Fermi surface of caesium.<sup>56</sup> In the present work, as well as in Ref. 23, the calculated Fermi surface is open around the *N* point and forms a belly—neck structure similar to the noble metals. It is, however, well known from experiments that the Fermi surface of caesium is closed and distorted from a sphere with a radial distortion of approximately 7%.<sup>57</sup> The present calculation also gives poor agreement for Cs regarding the total susceptibility, as presented in an earlier section. The origin of the failure of the LDA is not obvious. Due to this mismatch between theory and experiments for Cs, no attempt has been made to perform calculations of the ZS on the Fermi surface in the present work as the results would be very unreliable. A hint to the behavior in Cs can be found by studying the results in Ref. 23 where cyclotron orbits for lower energies than the Fermi energy, in order to make closed orbits, have been studied. In Ref. 23 studies of the heavier and, due to radioactivity, unstable metal francium are also presented.

The calculated values of *R* and *g<sub>c</sub>* and the amount of anisotropy for the rest of the alkali metals, using the BH potential, are presented in Table X, together with the ex-

TABLE X. Calculated values of  $R$  and  $g_c$  using the BH potential with the external field in the [001] direction for the alkali metals are presented, together with the anisotropy and the experimental determination of the  $g_c$  factor.

Metal	$R$ [001]	$\frac{\Delta R}{R$ [001]	$g_c$ [001]	$\frac{\Delta g_c}{g_c$ [001]	$\frac{g_c$ [001]}{1 + \lambda_{e-ph}}	$g_c$ exp
		( $\times 10^{-2}$ )		( $\times 10^{-3}$ )		
Li	3.00	20	3.75	11	2.72	
Na	1.57	0.5	3.10	7	2.56	2.636 <sup>a</sup>
K	1.83	2	3.39	12	2.97	2.800 <sup>b</sup>
Rb	1.98	12	3.48	14	3.13	2.83 <sup>b</sup>

<sup>a</sup>Reference 1.

<sup>b</sup>Reference 2.

perimentally determined values. In order to compare  $g_c$  values electron-phonon effects must be taken into account, and therefore also the electron-phonon renormalized values are presented. The values of the coupling constants are from Ref. 23.

The agreement in  $g_c$  is very good for sodium, but discrepancies are getting larger when going from potassium to rubidium. The anisotropy of  $R$  found in the calculations originates almost only from the anisotropy of the cyclotron orbit mass in the two latter metals. No anisotropy of  $R$  (and hence  $g_c$ ) could be detected in the experiments, as the difference between the values from different experimental techniques was larger than the differences for different orientations of the samples. In Table XI  $R$  for a field in the [001] direction has been calculated using different XC potentials. Comparison with Table III shows that  $R$  scales approximately as the total susceptibility, and the potential giving best agreement with experiments is the VWN potential.

For more details on Fermi-surface properties of the alkali metals related to external magnetic fields, cf. Ref. 23.

### B. Platinum group metals

In the present work the fcc metals rhodium, palladium, iridium, and platinum have been studied. Palladium is presented in an earlier section of the present paper.

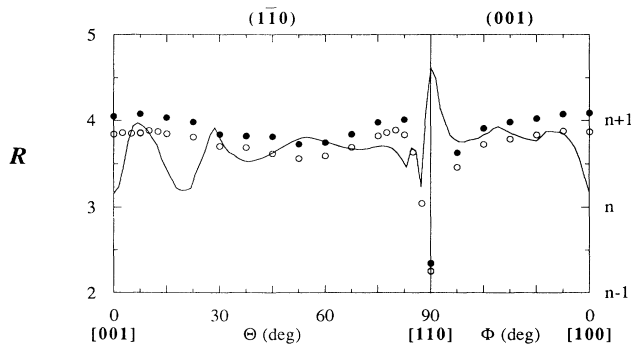


FIG. 9.  $R$  for orbits on the  $\Gamma_6$  sheet in Pt. Calculated values are presented with (full symbols) and without (empty symbols) OP. The experimental data (solid line) are from Ref. 18, and in the graph the arbitrary integer is chosen as 3.

Calculated and experimental<sup>18</sup> values of  $R$  on the  $\Gamma_6$  sheet in Pt are presented in Fig. 9. As can be seen in the graph the experimental data vary rapidly, while the only drastic behavior of the calculated data is near the [110] direction. The present calculations show a minimum in the [110] direction, as both theory and experiments do for the  $\Gamma_6$  sheet in Pd (cf. Fig. 2), while the experiments show a maximum. This could be due to a misinterpretation of the experimental data.<sup>58</sup>

On the  $\alpha$  orbit in Pt, presented in Fig. 10, the calculated anisotropic behavior is correct, but the calculations fall between two possible experimental curves. However, as seen in Table VII the total susceptibility is underestimated with a factor of 1.25. Enhancement of the calculated values with 1.25 then gives perfect agreement with experiments. For the  $\Gamma_6$  sheet a similar operation makes no substantial difference.

Similar to the situation for Pd (cf. Fig. 4) the agreement between theory and experiments for the  $X_4$  hole pocket is poor. As can be seen in Fig. 11, the experimental anisotropy<sup>19</sup> is much larger than the calculated one. In the experiments there is rotational symmetry, while the calculations show anisotropy in the (001) plane. This could be a consequence of the difficulty of calculating such a tiny Fermi-surface area correctly. In this case the calculated area is twice the size of the experimental one. Making the area smaller would contract it towards the  $X$  point, and the spherical asymmetry would then reduce. This is consistent with the experimental data for the  $X$  pocket in Pd (Fig. 4), which is larger than the corresponding surface in Pt, where anisotropy in the (001) plane is found.

It is also interesting to note that the inclusion of OP generally increases the ZS, except near [001] on the  $X$  pocket in Pt where a decrease is noted. This is a conse-

TABLE XI.  $R$  for the [001] direction calculated using different XC potentials.

Metal	$R$				Expt.
	BH	BHJ	VWN	GL	
Li	3.00	3.64	3.05	3.89	
Na	1.57	1.79	1.57	1.84	1.63
K	1.83	2.22	1.79	2.25	1.72
Rb	1.98	2.45	1.91	2.46	1.77

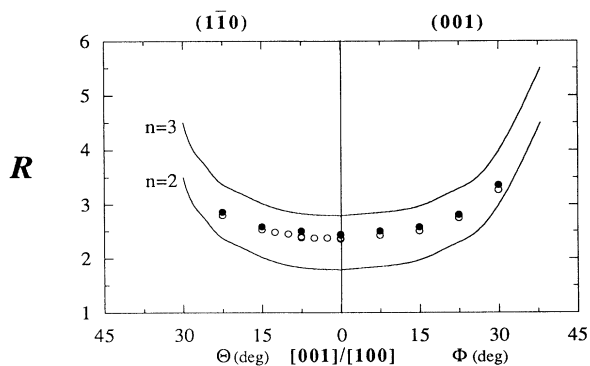


FIG. 10. Same as Fig. 9 but for the  $\alpha$  orbit in Pt. Two possible variations of the experimental data (Ref. 18) are plotted, with the arbitrary integers equal to 2 or 3.

quence of the negative orbital contribution to the ZS that is present also on the  $X$  pocket in Pd, (cf. Fig. 6). In Pt the enhancement of the orbital contribution from OP is large enough to decrease the total splitting.

In Table XII the influence of different XC potentials on  $R$  is presented, both for Pd and Pt. The trend of increasing splitting in the order BH, VWN, BHJ, and GL found in all systems studied is valid also for Pd and Pt, with exception for the  $X4$  pockets, where the orbital effects discussed above complicate the behavior.

Iridium has two  $\Gamma$ -centered electron sheets,  $\Gamma5$  and  $\Gamma6$ . The larger surface,  $\Gamma5$ , is difficult to study in dHvA experiments and therefore an experimental determination of the ZS exists only for the smaller surface. The calculated values of  $R$  for the two surfaces are presented in Fig. 12, together with the experimental variation for the  $\Gamma6$  surface.<sup>16</sup> However, it should be made clear that the interpretation of the experiments was done with the calculations in Ref. 20 as a guide. Similar to the Pt case, the experimental curve varies more than the calculated curves do.

On the larger one of the two  $X$  pockets,  $X4$ , the agreement between theory and experiment is satisfactory, as

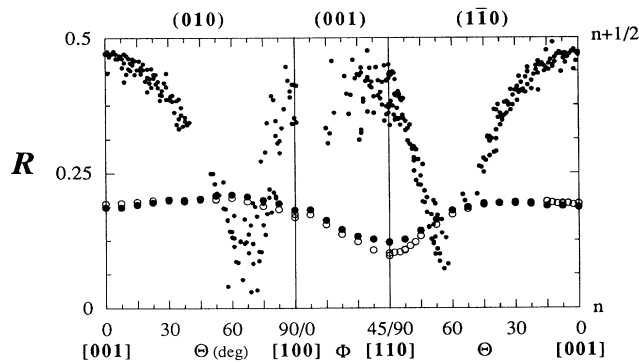


FIG. 11.  $R$  on the  $X$  hole pocket in Pt, calculated with (large solid circles) and without (empty circles) OP. Experimental data (small solid circles) are from Ref. 19. Any value of the unknown integer other than zero is very unlikely.

TABLE XII. Calculated values of  $R$  using different XC potentials for some orbits in Pd and Pt with the magnetic field in the  $[001]$  direction. For the  $X$  pockets two different orientations are possible.

Metal	Orbit	$R$			
		BH	BHJ	VWN	GL
Pd	$\Gamma6$	8.17	11.92	10.26	11.72
Pd	$\alpha5$	9.14	13.46	11.57	13.33
Pd	$X4 [001]$	1.54	2.35	2.00	2.38
Pd	$X4 [100]$	2.01	2.92	2.54	2.89
Pt	$\Gamma6$	4.05	4.35	4.24	4.43
Pt	$\alpha5$	2.43	2.61	2.55	2.68
Pt	$X4 [001]$	0.19	0.21	0.21	0.24
Pt	$X4 [100]$	0.18	0.19	0.18	0.19

can be seen in Fig. 13. For the  $X3$  pocket, being a very small surface, the calculations are almost isotropic, while experiments indicate an increase around the belly of the pocket compared to the  $[001]$  direction.

For rhodium, the experimental data are limited to three spin-splitting zeros on the  $\Gamma6$  sheet,<sup>13</sup> presented in Fig. 14 together with calculated values for the  $\Gamma6$  and  $\Gamma5$  sheets. The two spin-splitting zeros near  $30^\circ$  away from  $[001]$  do not fit in the theoretical behavior. For completeness,  $R$  on the  $X3$  and  $X4$  surfaces from the present work are presented in Fig. 15 although no comparison with experiment is possible.

As can be seen in Table XIII, the effect of using different XC potentials is similar to Pd and Pt. The only exception is the  $\Gamma5$  sheet in Ir, where the BHJ potential gives the largest value.

### C. Noble metals

A comparison of the ZS from dHvA measurements (for Cu Refs. 4, 5, and 6, for Ag Refs. 4 and 6, and for Au Refs. 4 and 6–9) and the present calculations for the noble metals, presented in Figs. 16, 17, and 18, first reveals that the calculated values generally are too large. How-

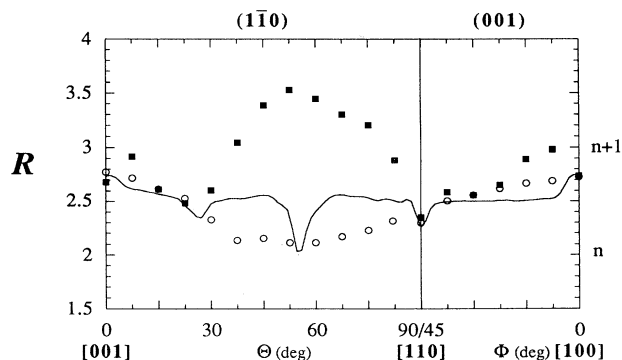


FIG. 12. Calculated values of  $R$  on the  $\Gamma5$  (squares) and  $\Gamma6$  (circles) Fermi-surface sheets in iridium. The experimental variation for the  $\Gamma6$  sheet (Ref. 16), placed around the integer 2, is also presented (solid line).

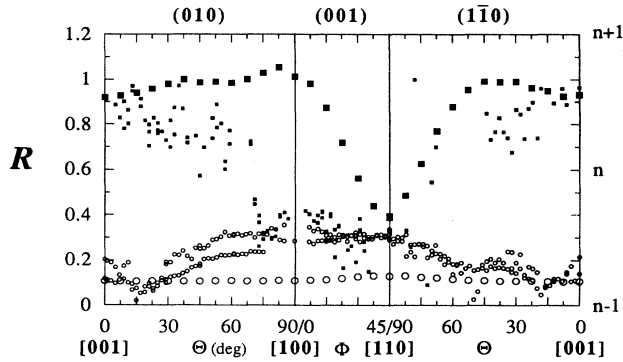


FIG. 13. Calculations and experiments (Ref. 17) for the  $X3$  and  $X4$  hole pockets in Ir. The  $X4$  pocket is marked with squares and the  $X3$  pocket with circles. Calculational data are presented with larger symbols, and the experiments with smaller symbols.

ever, the overall error is not as large as in the estimation of the susceptibility (cf. the preceding section). The anisotropic behavior is in good agreement with experiments. The belly orbit shows little anisotropy, while the neck orbit shows a pronounced “U shape.” The neck orbit in gold also shows the same behavior, but if the  $g_c$  factor is studied the theoretical curve turns “up-side down,” while the experiments show a minimum in [111]. The reason for this is that the cyclotron mass increases rapidly when the field direction is moved from the [111] direction, and the experimental estimation of  $R$  shows a more anisotropic behavior than the calculations do. This serves as an example of why it is advantageous to compare spin-splitting factors (i.e.,  $R$ ) from theory and experiments, rather than the  $g_c$  factors. The dog’s bone and rosette orbits all show a “parabolic” increase in  $R$  as the field is moved from the symmetry directions. This is similar to the behavior on the  $\alpha$  orbits in Pd and Pt, and is mostly due to an increasing mass, while the  $g_c$  factor is

TABLE XIII. Various XC potentials have been used for calculations of  $R$  for some Fermi-surface sheets with the field in the [001] direction in Rh and Ir.

Metal	Orbit	$R$			
		BH	BHJ	VWN	GL
Rh	$\Gamma5$	5.25	5.45	5.38	5.62
Rh	$\Gamma6$	3.72	3.84	3.77	3.86
Rh	$X3$ [001]	0.32	0.34	0.33	0.35
Rh	$X3$ [100]	0.41	0.44	0.42	0.44
Rh	$X4$ [100]	1.85	1.92	1.89	1.95
Rh	$X4$ [001]	1.58	1.66	1.63	1.66
Ir	$\Gamma5$	2.68	2.79	2.70	2.77
Ir	$\Gamma6$	2.77	2.76	2.76	2.80
Ir	$X3$ [001]	0.11	0.11	0.11	0.11
Ir	$X3$ [100]	0.11	0.12	0.11	0.12
Ir	$X4$ [100]	1.01	1.03	1.03	1.05
Ir	$X4$ [001]	0.93	0.94	0.93	0.94

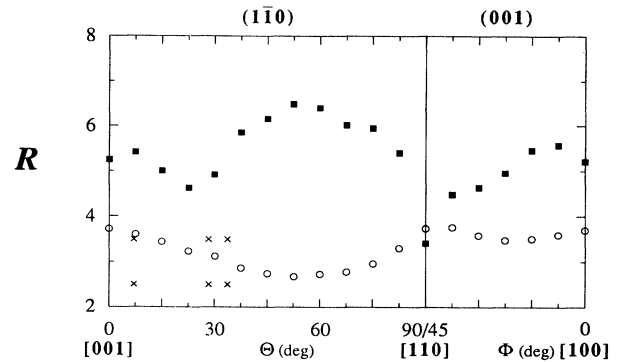


FIG. 14.  $\Gamma6$  and  $\Gamma5$  in rhodium. The experimentally determined (Ref. 13) spin-splitting zeros, corresponding to a value of  $R$  that is an integer plus one-half is marked with  $x$ .

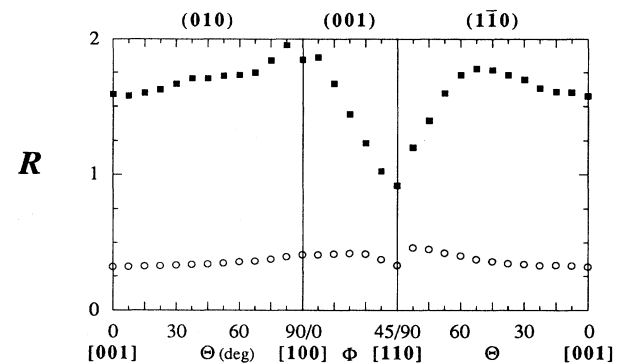


FIG. 15.  $R$  on the  $X4$  (squares) and  $X3$  (circles) pockets in rhodium.

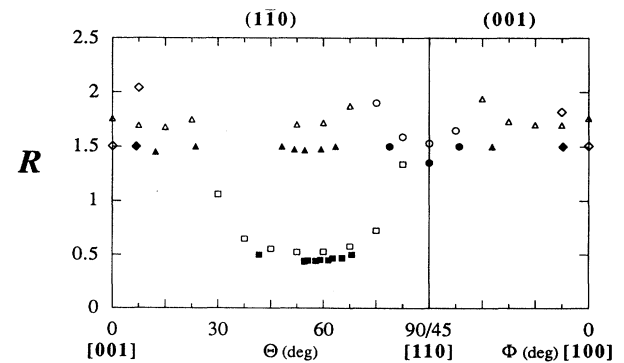


FIG. 16. Calculated (open symbols) and experimental (solid symbols) values of  $R$  in copper, for the belly orbit (triangles), dog’s bone orbit (circles), neck orbit (squares), and rosette orbit (diamonds). See text for references to experimental data.

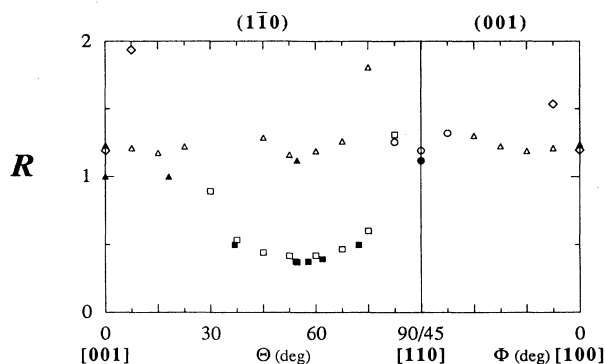


FIG. 17. Calculated (open symbols) and experimental (solid symbols) values of  $R$  in silver, for the belly orbit (triangles), dogs bone orbit (circles), neck orbit (squares), and rosette orbit (diamonds).

more or less constant.

In Table XIV the influence of the XC potential to the ZS in the noble metals is shown. As in previous systems, the GL potential gives the largest values, and the BH and VWN potentials give the lowest splittings.

### VIII. DISCUSSION AND CONCLUSIONS

The large contribution to the magnetization from the orbital moments in the late transition metals and the noble metals can easily be understood from a study of how the Zeeman Hamiltonian interacts with a model  $d$  band when spin splitting is small (i.e., not spontaneously spin-split metals) and spin-orbit coupling can be neglected. In that case spin and orbital splittings can be treated separately. The model  $d$  band will have a density of states at the Fermi level called  $D(E_F)$ , with equal weight in each of the 10 subbands,  $D = D(E_F)/10$ . The total spin moment (in Bohr magnetons) will then be the sum of the energy splitting times the density in each spin channel, i.e.,  $2\mu_B B \times 5D = \mu_B BD(E_F)$ , the Pauli spin susceptibility.

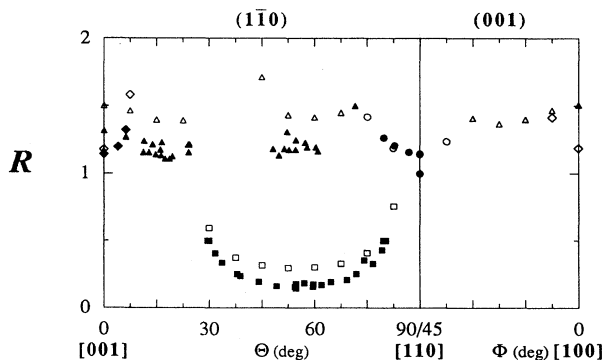


FIG. 18. Calculated (open symbols) and experimental (solid symbols) values of  $R$  in gold, for the belly orbit (triangles), dogs bone orbit (circles), neck orbit (squares), and rosette orbit (diamonds).

TABLE XIV. Calculated values of  $R$  for the [001] direction for the belly and rosette orbits in the noble metals, using the four different XC potentials.

Metal	Orbit	$R$			
		BH	BHJ	VWN	GL
Cu	belly	1.75	1.83	1.74	1.87
Cu	rosette	1.50	1.56	1.51	1.61
Ag	belly	1.23	1.29	1.25	1.30
Ag	rosette	1.19	1.24	1.21	1.27
Au	belly	1.50	1.51	1.50	1.53
Au	rosette	1.18	1.19	1.17	1.20

Exchange enhancement can be included by a factor  $S$ , and hence the total spin moment is  $10\mu_B BDS$ .

For the orbital moment a similar expression can be obtained. If the states with orbital quantum number  $+2$  and  $-2$  in one spin channel are considered we find that the difference in occupation for these two states are  $\mu_B B \times 4D$ , and their orbital moment will thus be  $\mu_B \times 8D$ . The states with  $m_l = -1$  or  $+1$  will similarly give  $\mu_B \times 2D$ . For the entire  $d$  band the orbital moment thus is  $20\mu_B BD$ . At this stage we might also include an orbital polarization enhancement factor,  $O$ , and the enhanced orbital moment is written  $20\mu_B BDO$ .

If we now consider the amount of orbital magnetization contributing to the total paramagnetic moment we find  $20\mu_B BDO / \mu_B BD(20O + 10S)$ . The orbital polarization enhancement is usually small. If also exchange enhancement is small as in the noble metals or iridium we can write  $S \approx O \approx 1$ , and find that the amount of orbital moment in a typical  $d$  band is  $\frac{20}{30}$ , or 67%. For a  $p$  or  $f$  band the corresponding values are  $\frac{4}{10}$  and  $\frac{56}{70}$ , or 40% and 80%, respectively. The corresponding values from the self-consistent calculations, also including spin-orbit coupling, are presented in Table VI. For Ir, where  $S$  is close to 1 and the state density at the Fermi level is dominated by  $d$  electrons, the self-consistently calculated amount of orbital moment is indeed large, 55%. However, Ir is a quite heavy atom where also spin-orbit coupling contributes to the orbital moment significantly. For the noble metals, a similar study requires that the amount of  $s$ ,  $p$ , and  $d$  character of the density of states at the Fermi level is taken into account, giving orbital contributions of 49%, 40%, and 48% for Cu, Ag, and Au, respectively. For gold, spin-orbit coupling can explain the difference between the simple estimate above and the value in Table VI. For silver the agreement is good while the orbital part is 7% too small in the estimate for copper. It should, however, be kept in mind that the self-consistently calculated total moments for the noble metals seem to be too large as compared to the experimental susceptibility.

For the systems studied here, with more than half-filled shells, the spin and orbital moments are always parallel, and both the spin-orbit coupling and the orbital part of the Zeeman operator contribute to the creation of the orbital magnetic moments. In the early transition metals

and the actinides, however, spin-orbit interaction tends to prefer an antiparallel arrangement while the Zeeman operator still aligns the moments in the same direction. The direction of the orbital magnetic moment will then be determined by the effect giving the largest energy gain. Preliminary self-consistent calculations for  $\alpha$ -Ce in a field of 10 T show that the spin and orbital moments are parallel, with values of 0.0017 and 0.0050 Bohr magnetons per atom, respectively.<sup>59</sup> This is consistent with the magnitude of the spin-orbit and orbital Zeeman energies, as the spin-orbit splitting parameter  $\xi$  in  $\alpha$ -Ce is 0.0742 eV, and thus  $\xi \langle l \rangle \langle s \rangle$  is smaller than  $\mu_B B \langle l \rangle$ .

It is always interesting to speculate in the possibilities to improve the current model. Even if the results in general show good agreement with experiments, and follow the trends from experimental data when going from one element to another, there are some drawbacks in the present results, and plenty of room for improvements. In the alkali metals Li and Cs show poor agreement, while Na, K, and Rb better follow the experiments. However, the results for the three latter metals could be expected to be even better than they are as they are thought of as "simple metals." MacDonald<sup>60</sup> has carried out detailed many-body calculations with three different approximations for the self-energy operator. His results indicate that in order to achieve a good agreement with experiment it is necessary to use a nonlocal and energy-dependent self-energy operator. The larger deviations in Li and Cs are explained by MacDonald as effects of an unusually large electron-electron renormalization. It is also well known that the LDA overestimates the bandwidths in the alkali metals in contrast to self-energy calculations.<sup>61,62</sup> Clearly the alkali metals should be treated in a model that is "beyond the LDA."

In the transition metals investigated here, the results are very good for Pd, while discrepancies are larger for Ir and Pt. For Rh the experimental situation is still not investigated, and comparisons are impossible. The failure of the present model in Pt is more difficult to understand than for the alkalis, as the band structure and Fermi surface are quite well described by the LDA. One way to improve the results could be to extend the basis set to also include  $f$  orbitals, which might be a way to provide the system with the possibility of an increased anisotropy. However, the  $f$ -projected density of states at the Fermi

level for the sixth band is only 1.5% of the total. In a later paper we will present calculations for Pt where also  $f$  orbitals are included. It is also possible that the muffin-tin approximation reduces the anisotropy. Previous investigations<sup>63</sup> of the contribution from non-muffin-tin terms to the potential show that the  $5d$  angular wave functions are well mixed in the metallic state and anisotropic effects in the potential are averaged out when calculating single-particle energies. This cancellation of the anisotropic contributions might not occur for the Zeeman splitting, which would result in larger anisotropy. Hence, we might have an explanation why the Fermi-surface anisotropy is better described than the anisotropy of the Zeeman splitting. This question can be sorted out by a full potential calculation. It is also possible that discrepancies occur when comparing calculations and experiments, as the LDA Fermi surface can be different from the physical one.<sup>32</sup> Finally, in the noble metals the anisotropy of the Zeeman splitting shows good agreement with experiments, but the splitting is approximately 10–20 % too large.

It is obvious that the most rigorous approach when an external magnetic field is present would be an implementation of current-density-functional theory, where it also could be possible to include the Landau condensation and diamagnetism in a band calculation *a priori*.<sup>31</sup> From what is stated above it is also evident that a local-density approximation is not sufficient. A realization of a nonlocal current-density-functional model with no shape restrictions on the potential would be very interesting to use for studies of the electronic structure of metals in external magnetic fields.

With these facts in mind, it is surprising that the results from the model described in the present paper are as good as they are.

#### ACKNOWLEDGMENTS

We are thankful for interesting discussions with Olle Eriksson, Lars Nordström, Per Söderlind, Joakim Trygg, and especially Lukas Severin for letting us use his computer code for magnetic form-factor calculations. This work has been financially supported by the Swedish Natural Science Research Council.

<sup>1</sup>J. M. Perz and D. Shoenberg, *J. Low-Temp. Phys.* **25**, 275 (1976).

<sup>2</sup>B. Knecht, *J. Low-Temp. Phys.* **21**, 619 (1975).

<sup>3</sup>M. Springford, I. M. Templeton, and P. T. Coleridge, *J. Low-Temp. Phys.* **53**, 563 (1983).

<sup>4</sup>D. L. Randles, *Proc. R. Soc. London, Ser. A* **331**, 85 (1972).

<sup>5</sup>P. T. Coleridge, G. B. Scott, and I. M. Templeton, *Can. J. Phys.* **50**, 1999 (1972).

<sup>6</sup>W. M. Bibby and D. Shoenberg, *J. Low-Temp. Phys.* **34**, 659 (1979).

<sup>7</sup>G. W. Crabtree, L. R. Windmiller, and J. B. Ketterson, *J.*

*Low-Temp. Phys.* **20**, 655 (1975).

<sup>8</sup>H. Alles, R. J. Higgins, and D. H. Lowndes, *Phys. Rev. B* **12**, 1304 (1975).

<sup>9</sup>G. W. Crabtree, L. R. Windmiller, and J. B. Ketterson, *J. Low-Temp. Phys.* **26**, 755 (1977).

<sup>10</sup>J. M. Perz, *Can. J. Phys.* **55**, 356 (1977).

<sup>11</sup>V. E. Startsev, P. T. Coleridge, I. M. Templeton, E. Fawcett, C. Muir, and J. M. Perz, *J. Low-Temp. Phys.* **55**, 175 (1984).

<sup>12</sup>O. Z. Ostapiak, J. M. Perz, V. Pluzhnikov, and V. E. Startsev, in *Proceedings of the International Conference on the Physics of Transition Metals, Darmstadt, 1992*, edited by P. M. Op-

- peneer and J. Kübler (World Scientific, Singapore, 1993), p. 244.
- <sup>13</sup>H. Ohlsén, P. Gustafsson, and L. Nordborg, *J. Phys. F* **16**, L79 (1986).
- <sup>14</sup>H. Ohlsén, P. Gustafsson, L. Nordborg, and S. P. Hörnfeldt, *Phys. Rev. B* **29**, 3022 (1984).
- <sup>15</sup>H. Ohlsén, P. Gustafsson, and L. Nordborg, *J. Phys. F* **16**, 1681 (1986).
- <sup>16</sup>P. Gustafsson, H. Ohlsén, and L. Nordborg, *J. Phys. F* **17**, 117 (1987).
- <sup>17</sup>A. Hjelm, L. Nordborg, and H. Ohlsén, *Phys. Rev. B* **41**, 7446 (1990).
- <sup>18</sup>P. Gustafsson, H. Ohlsén, and L. Nordborg, *Phys. Rev. B* **33**, 3749 (1986).
- <sup>19</sup>A. Hjelm, H. Ohlsén, and L. Nordborg, *Phys. Rev. B* **36**, 4647 (1987).
- <sup>20</sup>H. Ohlsén and J. L. Calais, *Phys. Rev. B* **35**, 7914 (1987).
- <sup>21</sup>O. Eriksson, H. Ohlsén, and J. L. Calais, *Phys. Rev. B* **40**, 5961 (1989).
- <sup>22</sup>G. E. Grechnev, N. V. Savchenko, I. V. Svechkarov, M. J. G. Lee, and J. M. Perz, *Phys. Rev. B* **39**, 9865 (1989).
- <sup>23</sup>A. Hjelm and J. L. Calais, *J. Magn. Magn. Mater.* **110**, 275 (1992).
- <sup>24</sup>A. Hjelm and J. L. Calais, *Phys. Rev. Lett.* **67**, 2064 (1991).
- <sup>25</sup>P.-O. Löwdin, *J. Mol. Spectrosc.* **14**, 131 (1964).
- <sup>26</sup>G. Vignale, M. Rasolt, and D. J. W. Geldart, *Adv. Quantum Chem.* **21**, 235 (1990).
- <sup>27</sup>W. Kohn and P. Vashishta, in *Theory of the Inhomogeneous Electron Gas*, edited by S. Lundqvist and N. H. March (Plenum, New York, 1983).
- <sup>28</sup>G. Vignale and M. Rasolt, *Phys. Rev. Lett.* **59**, 2360 (1987).
- <sup>29</sup>G. Vignale and M. Rasolt, *Phys. Rev. B* **37**, 10 685 (1988).
- <sup>30</sup>E. Brown, *Solid State Physics* **22**, 313 (1968).
- <sup>31</sup>J. W. Serene, *Phys. Rev. B* **39**, 13 206 (1989).
- <sup>32</sup>D. Mearns, *Phys. Rev. B* **38**, 5906 (1988).
- <sup>33</sup>D. Shoenberg, *Magnetic Oscillations in Metals* (Cambridge University Press, Cambridge, 1984).
- <sup>34</sup>S. Engelsberg and G. Simpson, *Phys. Rev. B* **2**, 1657 (1970).
- <sup>35</sup>H. L. Skriver, *The LMTO Method* (Springer-Verlag, Berlin, 1984).
- <sup>36</sup>O. Eriksson, M. S. S. Brooks, and B. Johansson, *Phys. Rev. B* **41**, 7311 (1990).
- <sup>37</sup>O. Eriksson, B. Johansson, R. C. Albers, A. M. Boring, and M. S. S. Brooks, *Phys. Rev. B* **42**, 2707 (1990).
- <sup>38</sup>U. von Barth and L. Hedin, *J. Phys. C* **5**, 1629 (1972).
- <sup>39</sup>A. P. Cracknell, *J. Phys. C* **2**, 1425 (1969).
- <sup>40</sup>M. S. S. Brooks and P. J. Kelly, *Phys. Rev. Lett.* **51**, 1708 (1983).
- <sup>41</sup>R. Ahuja, A. K. Solanki, and S. Auluck, *Phys. Status Solidi* **160**, 549 (1990).
- <sup>42</sup>R. Ahuja, A. K. Solanki, and S. Auluck, *Phys. Status Solidi* **168**, 509 (1991).
- <sup>43</sup>R. Ahuja, A. K. Solanki, T. Nautiyal, and S. Auluck, *Pramana J. Phys.* **32**, 831 (1989).
- <sup>44</sup>J. F. Janak, V. L. Moruzzi, and A. R. Williams, *Phys. Rev. B* **12**, 1257 (1975).
- <sup>45</sup>O. Gunnarsson and B. I. Lundqvist, *Phys. Rev. B* **13**, 4274 (1976).
- <sup>46</sup>S. H. Vosko, L. Wilk, and M. Nusair, *Can. J. Phys.* **58**, 1200 (1980).
- <sup>47</sup>G. H. O. Daalderop, P. J. Kelly, and M. F. H. Schuurmans, *Phys. Rev. B* **41**, 11 919 (1990).
- <sup>48</sup>J. W. Cable, E. O. Wollan, G. P. Felcher, T. O. Brun, and S. P. Hörnfeldt, *Phys. Rev. Lett.* **34**, 278 (1975).
- <sup>49</sup>W. Marshall and S. W. Lovesey, *Theory of Thermal Neutron Scattering* (Oxford University Press, Oxford, 1971).
- <sup>50</sup>R. Maglic, T. O. Brun, G. P. Felcher, and Y. K. Chang, *J. Magn. Magn. Mater.* **9**, 318 (1978).
- <sup>51</sup>N. W. Ashcroft and N. D. Mermin, *Solid State Physics* (Saunders, Philadelphia, 1988).
- <sup>52</sup>M. Singh, J. Callaway, and C. S. Wang, *Phys. Rev. B* **14**, 1214 (1976).
- <sup>53</sup>P. K. Misra and L. M. Roth, *Phys. Rev.* **177**, 1089 (1969).
- <sup>54</sup>R. E. Peierls, *Quantum Theory of Solids* (Oxford University Press, Oxford, 1955).
- <sup>55</sup>I. V. Svechkarov, V. I. Poltoratskii, and L. F. Mar'yanina, *Fiz. Tverd. Tela (Leningrad)* **17**, 1987 (1975) [*Sov. Phys. Solid State* **17**, 1299 (1976)].
- <sup>56</sup>See, e.g., M. J. Lawrence, *J. Phys. F* **1**, 836 (1971).
- <sup>57</sup>A. A. Gaertner and I. M. Templeton, *J. Low-Temp. Phys.* **29**, 205 (1977).
- <sup>58</sup>S. P. Hörnfeldt (private communication).
- <sup>59</sup>A. Hjelm (unpublished).
- <sup>60</sup>A. H. MacDonald, *J. Phys. F* **10**, 1737 (1980).
- <sup>61</sup>J. E. Northrup, M. S. Hybertsen, and S. G. Louie, *Phys. Rev. B* **39**, 8198 (1989).
- <sup>62</sup>M. P. Surh, J. E. Northrup, and S. G. Louie, *Phys. Rev. B* **38**, 5967 (1988).
- <sup>63</sup>A. H. MacDonald, J. M. Daams, S. H. Vosko, and D. D. Koelling, *Phys. Rev. B* **23**, 6377 (1981).